CHEMISTRY OF MATERIALS

Article

pubs.acs.org/cm

Interface Control of Photoelectrochemical Water Oxidation Performance with $Ni_{1-x}Fe_xO_y$ Modified Hematite Photoanodes

Hamed Hajibabaei, Abraham R. Schon, and Thomas W. Hamann*

Department of Chemistry, Michigan State University, East Lansing, Michigan 48824-1322, United States

Supporting Information

ABSTRACT: In this work, $Ni_{1-x}Fe_xO_y$ coated hematite electrodes are investigated as a model system of different semiconductor/catalyst interfaces. We found that the photoelectrochemical (PEC) performance of the electrodes strongly depends on both the way the hematite electrode is prepared and the composition of the catalyst. Two extreme behaviors are observed for electrodeposited hematite electrodes coated with different compositions of catalyst. In the case of Fe-rich catalyst ($Ni_{0.25}Fe_{0.75}O_y$), the performance is substantially enhanced compared to the bare electrode; however, the Ni-rich ($Ni_{0.75}Fe_{0.25}O_y$) catalyst inhibits the PEC performance. A combination of photoelectrochemical, intensity modulated photocurrent spectroscopy, and electrochemical impedance spectroscopy measurements collectively reveal the critical role that the interface states of the semiconductor and catalyst plays in controlling the key interfacial charge transfer and recombination reactions. The photogenerated holes are efficiently collected and stored into the catalyst layer for the $Ni_{0.25}Fe_{0.75}O_y$ coated hematite electrodes. An unusually large improvement in performance is attributed to this hole collection circumventing recombination at the hematite surface. For the $Ni_{0.75}Fe_{0.25}O_y$ coated hematite electrodes, however, there is a presence of interface trap states that act as recombination centers and pin the catalyst potential. These combined results provide important new understanding of the role of the interfaces at semiconductor/electrocatalyst junctions.

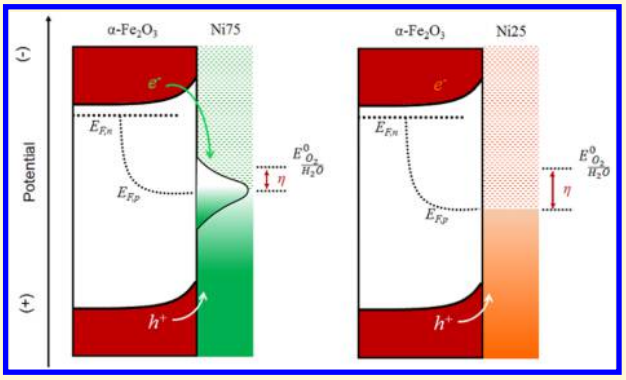

INTRODUCTION

Hematite continues to attract a lot of interest as an electrode material for photoelectrochemical (PEC) water oxidation. Hematite has an optical band gap of ~2.1 eV, is composed of very earth abundant elements, is easily prepared, and is chemically stable in basic electrolytes.[1−3] Because of these attributes, there has been a lot of effort aimed at improving the performance of this material. Previous studies suggest that one of the key steps preventing efficient PEC water oxidation at hematite electrode is the high overpotential necessary to initiate water oxidation.[3,4] The large overpotential is generally attributed to the slow kinetics of water oxidation at the surface of the hematite. Experiments by us and others showed that after deposition of water oxidation catalysts (WOCs), e.g., CoPi or $Ni(OH)_2$, the photoelectrode characteristics (e.g., photocurrent onset potential, photocurrent, and fill-factor) substantially improve.[2,5−11] The cause for these improvements, however, are not yet fully understood. The enhancement of PEC performance of electrocatalyst coated photoanodes has been attributed to reducing surface state recombination,[12,13] increasing band bending,[14,15] or facilitating charge separation.[10,16] Recently, Boettcher and co-workers developed a dual working electrode experiment to simultaneously measure the current and potential of the semiconductor (SC) and catalyst.[17,18] Their results suggest that the SC/WOC interface is strongly affected by the physical structure of the catalyst, specifically whether it is dense or ion permeable. To the best of our knowledge, all catalysts reported in conjunction with hematite are ion permeable, including the most often reported Co-Pi.[9] For such ion permeable WOCs, hole transfer from the semiconductor oxidizes the WOC, and the accumulated holes are charge compensated by ions in the electrolyte. Thus, the catalyst potential drops until it can sustain water oxidation at a rate matching the flux of holes reaching the SC/WOC interface. This type of junction is termed an adaptive junction.

The adaptive junction model assumes an ideal SC/WOC interface and the measurements reported by Boettcher utilized an ideal single crystal TiO_2 semiconductor that does not appear to significantly suffer from surface state recombination. We have shown, however, that surface states on hematite largely control the water oxidation behavior and cannot necessarily be neglected in considering the addition of WOC's to the hematite surface.[19,20] For example, it was shown that surface modification of hematite by removing the surface defects, resulted in a substantial improvement of PEC performance of hematite electrodes modified with WOC's.[21] In addition, it has been reported that many other photoanode materials such as and $BiVO_4$ suffer from surface state recombination as well.[22,23]

Received: March 21, 2017
Revised: July 17, 2017
Published: August 8, 2017

DOI: 10.1021/acs.chemmater.7b01149
Chem. Mater. 2017, 29, 6674−6683

The presence of a high density of surface states can result in substantial surface state recombination and pin the Fermi level.[9,24] Their influence on the interface that forms upon addition of a WOC is unknown, however. Further, the addition of materials to the hematite (and other metal oxide) surfaces can result in new/more interface states that can inhibit the performance. It is also not clear why some hematite/WOC junctions produce exceptional results, compared to most other junctions that result in modest improvements.[21,25,26] Therefore, in this study we aim to expand the understanding of SC/WOC interfaces, including nonideal junctions, which can be further generalized for a larger groups of photoelectrode/WOCs combinations.

In this work, we employ hematite thin films prepared by atomic layer deposition (ALD) and electrodeposition (ED) methods as photoanodes. Recently, we have shown that the preparation method of hematite has a great impact on the performance of the photoanode.[2] The ED hematite electrodes outperformed the ALD-made films, which was attributed to an enhanced hole transport and collection efficiency. Therefore, it is expected that the density of defects at the surface may also be altered as a result of different preparation method. The hematite films were coated with $Ni_{1-x}Fe_xO_y$ WOCs. Consistent with prior reports, we found that tuning the composition of the $Ni_{1-x}Fe_xO_y$ catalysts results in formation of one or two separate phases including FeOOH and Fe-doped NiOOH.[27−30] Thus, a combination of hematite electrodes prepared by different methods and $Ni_{1-x}Fe_xO_y$ WOCs provides a good system for studying the role of the interface formed at the SC/WOC junction. The $Ni_{1-x}Fe_xO_y$ coated hematite electrodes were studied using electrochemical impedance spectroscopy (EIS) and intensity modulated photocurrent spectroscopy (IMPS) as a function of composition of the catalysts to determine the factors controlling the performance of the modified electrodes. These combined results provide new insight of the SC/WOC junction and allow for further development of more efficient solar water splitting systems.

EXPERIMENTAL SECTION

Thin films of hematite electrodes were prepared on F:SnO_2 (FTO)-coated aluminoborosilicate glass substrates (Solaronix, 10 Ω/sq) via electrodeposition (ED) and atomic layer deposition, (ALD) methods reported previously.[2,31] Prior to deposition, the FTO glass was cleaned by ∼15 min sequential sonication in soap, water, and isopropyl alcohol and dried in a gentle stream of nitrogen. The ED of planar thin films were performed in 0.1 M $FeCl_2{\cdot}4H_2O$ (pH = ∼4.2) at 60 °C by applying 1.2 V vs. Ag/AgCl reference electrode under gentle stirring for 30 min. Subsequently, the amorphous electrodeposited FeOOH films were converted to crystalline hematite by annealing at 800 °C in a preheated furnace for 10 min followed by quenching to the room temperature. Analogous thicknesses of hematite were deposited via ALD on a ∼2 nm Ga_2O_3 underlayer. The Ga_2O_3 was deposited using tris(dimethylamido)gallium(III) ($Ga_2(NMe_2)_6$) (Strem Chemicals Inc.) as the Ga precursor and H_2O as the oxidant using a modified version of previously reported procedure.[32] The Ga cylinder was heated to 150 °C and pulsed for 0.2 s under exposure mode for 8 s, followed by 12 s purge. Then, a 0.015 s pulse of H_2O was introduced under the same exposure-purge time to oxidize the Ga precursor. A growth rate of ∼1.1 Å Ga_2O_3/cycle was measured by spectroscopic ellipsometry (Horiba Jobin Yvon, Smart-SE) on control Si wafers. The Ga_2O_3 coated FTO substrates were subsequently coated with the ∼30 nm of Fe_2O_3 by alternating pulses of ferrocene as iron precursor and a combination of water and ozone as the oxidant. The ferrocene cylinder, heated to 70 °C, was pulsed for 20 s, and was followed by an oxidation cycle that included 10 subcycles of a 0.015 s H_2O pulse followed by a 2 s ozone pulse, where each subcycle was separated by a 5 s purge. In agreement with our previous report, the growth rate of Fe_2O_3 is 0.55 Å/cycles.[33] After deposition, the ALD Fe_2O_3 films were annealed at 500 °C for 2 h with heating/cooling rate of 17 °C/min. Finally, the electrodes were annealed in a preheated furnace at 800 °C for 4 min.

Thin films of $Ni_{1-x}Fe_xO_y$ were deposited by spin coating on 1 cm^2 FTO and hematite substrates using a modified version of previously reported procedures.[21,34] Prior to the deposition of the catalyst on FTO, the substrates were sequentially cleaned by sonication in soap, DI water, and IPA for 15 min. To coat the hematite electrodes with catalyst, the freshly prepared hematite electrodes were only rinsed with DI water followed by drying in a stream of N_2. Precursor solutions were prepared from iron(III) 2-ethylhexanoate (50% w/w in mineral spirits, Strem Chemicals), and nickel(II) 2-ethylhexanoate (78% w/w in 2-ethylhexanoic acid, Strem Chemicals) by dissolving the appropriate amount of metal precursor in hexanes (Table S1) to give a total concentration of 15% w/w metal complex. These solutions were further diluted with hexane to prepare a solution with a total metal concentration of 50 mM. Approximately 0.25 mL of the solution was added to the substrate, followed by spinning at 5000 rpm for 60 s. Subsequently, the films were irradiated with UV light (254 nm, 4 W) for 1 h followed by annealing in a preheated furnace in air at 100 °C for 1 h. We used Raman spectroscopy to ensure that the decomposition of organic precursor was completed (Figure S1). To change the thickness of the catalyst, the deposition procedure was performed 1, 2, or 3 times sequentially to produce three thicknesses of catalysts on the ED hematite electrodes. Note that each deposition cycle involved 1 h of UV light treatment followed by 1 h of annealing at 100 °C. Atomic force microscopy (AFM) and spectroscopic ellipsometry (SE) were utilized to determine the thickness of the catalyst deposited on silicon substrates using comparable procedures. A wavelength region of 800−1000 nm was used for SE measurements because the oxides are transparent, which allows for more accurate determination of thickness.[35]

X-ray photoelectron spectroscopy (XPS) was utilized to determine the composition of the thin films of $Ni_{1-x}Fe_xO_y$ catalyst on FTO. The XPS data were collected utilizing PerkinElmer Phi 5600 ESCA system equipped with a monochromatic Mg Kα source to illuminate the sample at a takeoff angle of 45°. Survey scans of 0−1000 eV binding energy and detailed scans for C 1s, O 1s, Ni 2p, and Fe 2p regions were measured for all samples. The binding energies were corrected in reference to C 1s peak (284.8 eV) and Shirley background subtraction was performed for fitting for each sample. For fitting the Ni and Fe 2p regions, the p1/2 and p3/2 peaks were bonded together with the relative area of 1 to 2. Raman spectra were collected via Raman Microprobe (Renishaw) equipped with a 45W Cobalt DPSS laser (532 nm line) laser and a 100× mag. objective to focus the laser on the film surface. The surface morphology of the prepared films were examined by scanning electron microscopy, SEM (Carl Zeiss Auriga, Dual Column FIBSEM).

Electrochemical measurements were made with an Eco Chemie Autolab potentiostat coupled with Nova electrochemical software. The electrochemical characterization of $Ni_{1-x}Fe_xO_y$ on FTO was carried out by cycling the potential linearly between 1.0 and 2.0 V vs RHE at a scan rate of 100 mV s^{-1}. The electrodes were examined in contact with 1 M KOH solution (pH = 13.6) as was determined with Fisher Scientific Accument pH meter. Each electrode was activated by cycling the potential between 1 and 2 V vs RHE (40 CVs). All the presented CVs are measured after activation. The potential was corrected for IR drop, using R values determined by impedance measurements. A homemade saturated Ag/AgCl and a platinum mesh electrodes were used as the reference and counter electrodes, respectively. The reference electrode was frequently calibrated against commercial saturated calomel electrode (Koslow Scientific). All the potentials were converted to reversible hydrogen electrode, RHE, by equation $E_{RHE} = E_{Ag/AgCl} + 0.197\ V + (0.059\ V) \times pH$.

The electrochemical impedance spectroscopic and photoelectrochemical measurements were made with an Eco Chemie Autolab potentiostat coupled with Nova electrochemical software. Impedance

DOI: 10.1021/acs.chemmater.7b01149
Chem. Mater. 2017, 29, 6674−6683

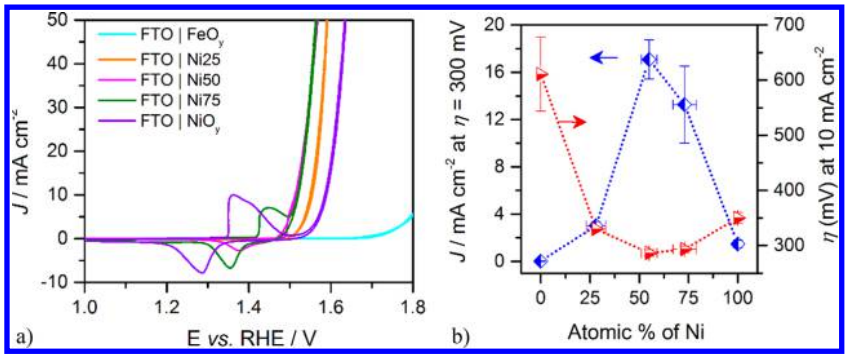

Figure 1. (a) IR-corrected CVs of $Ni_{1-x}Fe_xO_y$ catalysts on FTO substrates; FeO_y (cyan), $Ni_{0.25}Fe_{0.75}O_y$ (orange), $Ni_{0.5}Fe_{0.5}O_y$ (pink), $Ni_{0.75}Fe_{0.25}O_y$ (green), and NiO_y (purple). (b) Plots of current density at 300 mV overpotential (blue diamonds) and overpotential at 10 mA cm^{-2} (red triangle) as a function of the % Ni in contact with 1 M KOH; the compositions, activities, and the error bars are the average and standard deviations acquired from three independently prepared samples.

data were gathered using a 10 mV amplitude perturbation of between 10 000 and 0.01 Hz. Data were fit using Zview software (Scribner Associates). For each thickness of catalyst with different compositions, two electrodes were prepared and the fitted parameters were averaged and the standard deviations were reported on the graphs. The current density vs applied potential (J–E) response of bare and modified hematite electrodes were examined by cycling the potential between −0.5 and +0.7 V vs. Ag/AgCl at the scan rate of 20 mV s^{-1} in contact with 1 M KOH. The light source was a 450 W Xe arc lamp (Horiba Jobin Yvon). An AM 1.5 solar filter was used to simulate sunlight at 100 mW cm^{-2} (1 sun). Unless otherwise stated, all photoelectrochemical tests were carried out by shining light on the electrodes through the electrolyte.

The performance of each electrode was initially tested by measuring the J–E in light and dark. Subsequently, each electrode was conditioned by cycling between 0.5 and 1.7 V vs. RHE under illumination, followed by another J–E measurement. Each electrode was then subjected to EIS (∼2 h under illumination) and IMPS (∼1 h under illumination) measurements, with additional J–E measurements after EIS and IMPS measurements to determine any change in behavior. Negligible changes were observed between initial (after conditioning/before EIS) and final J–E curves for a given electrode. The J–E data shown are from the final measurements.

IMPS measurements were made with an Eco Chemie Autolab potentiostat equipped with metrohm LED driver accessory that was controlled by Nova electrochemical software. The measurements were performed in 1 M KOH utilizing a three electrode configuration. A 470 nm LED light was utilized as the light source for all the experiment. The power of the LED was chosen in a way that it provided the same number of photocurrent as was measured under 1 sun illumination. The modulation intensity was set at 10% of the power of the LED to ensure a linear respond and the frequency was swept from 15 kHz to 0.1 Hz with 10 frequency per decade increments. The IMPS data were collected over the potential range of 0.5 to 1.5 V vs RHE with 0.1 V interval.

RESULTS AND DISCUSSION

XPS measurements were performed on five catalysts prepared with variable composition of the $Ni_{1-x}Fe_xO_y$ solution (x = 0, 0.25, 0.5, 0.75, and 1) on FTO substrates. The compositions of the films determined by XPS, summarized in Table S2, are in good agreement with the composition of the solutions used for spin coating. The detailed XPS spectra as a function of the composition of the films are shown in Figure S2, followed by interpretation of the spectral features. Depending on the ratio of Ni to Fe, $Ni_{1-x}Fe_xO_y$ may consist of one or more separate phases. For iron concentration up to 25% only one phase, presumably Fe-doped $Ni(OH)_2$, is discernible. At higher iron content, however, two phases appear to be present, which are assigned to FeOOH and Fe-doped $Ni(OH)_2$, in accord with recent studies on the electrocatalytic activity of $Ni_{1-x}Fe_xO_y$ on different substrates.[36] This observation suggests that by tuning the composition of the catalyst, the interface of the electrocatalyst and underlying substrate may be modified by contact with the different catalyst phases.

The cyclic voltammograms (CV) of the $Ni_{1-x}Fe_xO_y$ catalysts on FTO in contact with 1 M KOH are shown in Figure 1a. The CV of NiO_y exhibits two characteristic features: a redox wave which is attributed to the transition between $Ni(OH)_2$ and NiOOH, and an anodic wave at more positive potentials corresponding to water oxidation.[29,37,38] The CV of FeO_y, on the other hand, only shows an anodic wave associated with water oxidation.[29] Similar to the NiO_y catalyst, the CV of the $Ni_{1-x}Fe_xO_y$ catalysts shows two features: one redox wave for the transition from $Ni(OH)_2$ to NiOOH and an anodic wave due to water oxidation. Consistent with previous studies, the position and the area of the redox peaks are strongly correlated to the composition of the film.[27,38] As the Fe content increases the redox peak shifts to more positive potentials, at iron concentrations beyond 25% the redox peak was merged into the water oxidation wave and is no longer observable.[29,37,36] To compare the electrocatalytic activity of the $Ni_{1-x}Fe_xO_y$ catalysts, the current density at 300 mV overpotential and the overpotential required to produce 10 mA cm^{-2} were determined. A plot of these two parameters as a function of Ni (content determined by the XPS) is shown in Figure 1b. The maximum current density at 300 mV overpotential and the minimum overpotential required to achieve 10 mA cm^{-2}, i.e. the highest activity for oxygen evolution reaction (OER), were observed for the film with 75–50% nickel content. We note that the composition of the most active catalyst is comparable to previous reports where thin films of Ni–Fe catalysts were prepared by different methods on different substrates.[29,36,39]

The composition of the catalysts after electrochemical conditioning were studied via XPS (Table S2b). With the exception of the NiO_y catalyst, we did not observe a change in the composition of the catalysts after electrochemical conditioning. Iron was electrochemically intercalated into the NiO_y films, however, in agreement with prior studies.[29,38] Raman spectroscopy was used to investigate a possible phase change of the catalysts during conditioning; however, the catalysts prepared by this method are thin and amorphous and show no distinguishable peaks in agreements with other reports.[34,40,41]

DOI: 10.1021/acs.chemmater.7b01149
Chem. Mater. 2017, 29, 6674–6683

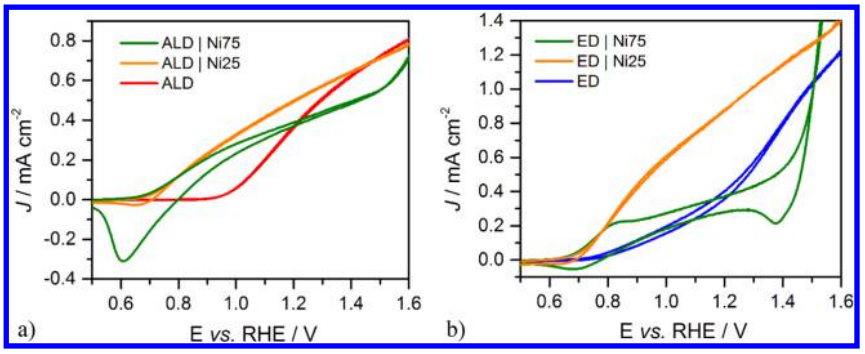

Figure 2. $J-E$ curves measured at 20 mV s^{-1} under 1 sun illumination for bare and modified (a) ALD and (b) ED hematite electrodes in contact with 1 M KOH solution; bare ALD (red), bare ED (blue), Ni75 coated hematite (green), Ni25 coated hematite (orange). The dark current are not included for the sake of clarity and are shown in Figure S8.

The influence of the electrocatalyst composition on the performance when integrated with hematite electrodes was further investigated. The hematite electrodes were prepared via ED and ALD. As shown by Raman and SEM, the morphology and crystallinity of the films remained unaffected after modification with catalyst (Figures S3 and S4). These observations indicate that the catalyst coating with this method is solely a surface modification with no alteration of the bulk characteristic of hematite.

The current density (J) vs applied potential (E) responses in the dark and under illumination of bare ED and ALD hematite electrodes, as well as ED and ALD electrodes modified with the five compositions of the $Ni_{1-x}Fe_xO_y$ catalysts are shown in Figure S5. Though no obvious change in the PEC water oxidation performance of the FeO_y coated electrodes were observed, the performance of both ED and ALD electrodes modified with NiO_y were substantially diminished. In addition, it was noted that for the ALD electrodes all three catalysts, i.e., Ni25, Ni50, and Ni75, resulted in ∼200 mV cathodic shift of the photocurrent onset potentials and thus improved performance. For the ED electrodes, on the other hand, only Ni25 improved the performance while Ni50 and Ni75, similar to the NiO_y, diminished the photocurrent response of the ED hematite electrode. To determine the underlying cause for the different behavior, two representative catalyst compositions were selected for more in-depth investigations described below: $Ni_{0.25}Fe_{0.75}O_y$ (Ni25) as the Fe-rich catalyst, and $Ni_{0.75}F_{0.25}O_y$ (Ni75) as the Ni-rich catalyst. To ensure the reproducibility of the behavior of the modified electrodes described below, $J-E$ measurements for several additional batches of electrodes prepared independently by different people on different days were performed. The $J-E$ curves for catalyst coated hematite electrodes are shown in Figures S6 and S7. The PEC behavior of the bare ALD electrodes is very consistent; however, there is some variability of the behavior of the bare ED electrodes. This is not too surprising given the different preparation methods. In both cases, however, the trend of performance and the effect of the different catalyst compositions is reproducible.

The dark $J-E$ curves Ni25 and Ni75 catalysts, are compared in Figure S8. The dark current behavior follows the same trends in activity as these catalysts on FTO, with increasing activity in the order Ni75 > Ni25 > bare. This result suggests that for the thin film of catalysts the electrocatalytic activates are nominally independent of the hematite substrate. Representative $J-E$ curves under illumination for the bare and modified electrodes are shown in Figure 2. Consistent with our prior report, the bare ED electrode somewhat outperformed the bare ALD electrode.[2] The effect of the different catalysts on the performance of the ED and ALD hematite electrodes is dramatically different, however. For the ALD hematite electrodes (Figure 2a), both catalyst compositions improved the performance. This result agrees with our prior studies that showed surface modification of ALD hematite electrodes by coating with Co-Pi or NiO_y enhanced the overall performance of the electrode by increasing charge separation from hematite to the catalyst at the surface, thereby suppressing surface recombination rates.[42,43] This behavior is generally consistent with the formation of an adaptive junction at SC/WOC interface.[17,42] In the case of Ni75 coated ALD electrode a capacitive peak prior to the water oxidation wave is clearly observable. This peak is generally observed for $Ni(OH)_2$ coated semiconductor electrodes, i.e., Fe_2O_3 or TiO_2, under PEC water oxidation conditions and it is attributed to the Ni^{3+}/Ni^{2+} redox reaction.[6,17]

For the ED hematite electrodes shown in Figure 2b, on the other hand, the $J-E$ responses are strongly dependent on the composition of the catalyst. For the Ni25 coated ED electrodes, a ∼300 mV negative shift of the photocurrent onset potential is produced. In addition, the photocurrent density and fill factors are significantly improved compared to the bare electrode. Conversely, for the Ni75 coated ED electrodes, the performance is suppressed. This behavior contrasts the electrocatalytic activity, where Ni75 outperforms Ni25. In addition to the diminished performance, the $J-E$ curve with Ni75 exhibits two well-separated capacitive features; a redox peak located at ∼0.7 V vs RHE, similar to the ALD electrodes, and a second peak at ∼1.35 V vs RHE. The first capacitive wave at ∼0.7 V vs RHE is assigned to charging of the catalyst film, which is generally seen for Ni-rich $Ni_{1-x}Fe_xO_y$ catalysts and is attributed to oxidation of Ni^{2+} to Ni^{3+}.[6] Figure S9 shows an increase in the magnitude of this wave in response to increasing incident light intensities from 0.1 sun to 3.5 suns, which further supports this assignment.

Because the dark $J-E$ curve of Ni75 on the ED electrodes (Figure S8) and the light $J-E$ curve of the bare ED electrodes both show very good activity, whereas the combination suppresses the performance, we hypothesize that deleterious interface states develop between the ED hematite and Ni75 catalyst films. Interestingly, because the ALD hematite electrode modified with the Ni75 catalyst exhibits good performance, the proposed development of Ni75/hematite interface states is not general, but appears to be a function of the particular hematite surface that is modified with the Ni75 catalyst. An additional control system was fabricated using a

DOI: 10.1021/acs.chemmater.7b01149
Chem. Mater. 2017, 29, 6674−6683

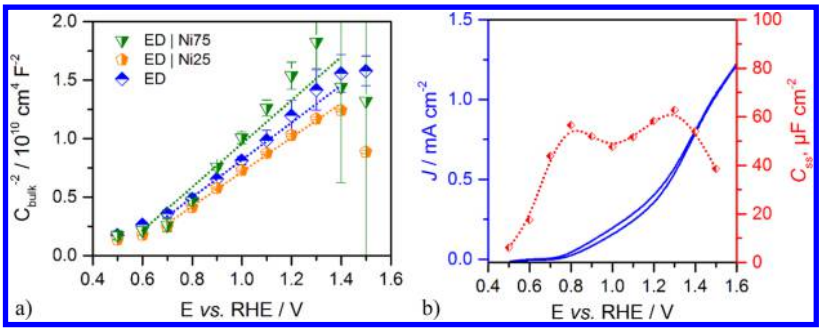

Figure 3. (a) MS plots for bare and catalyst modified ED electrodes, (b) J–E curve and C_{ss} values for bare ED electrode under 1 sun illumination in contact with 1 M KOH; bare electrode (blue diamond), Ni75 modified ED electrode (green triangle), and Ni25 coated ED electrode (orange pentagon). The dotted lines are the linear fitting used to extract the dopant density.

NiO_y catalyst, without the intentional incorporation of Fe, deposited on an ED electrode. The J–E curve of this system showed a redox wave with similar magnitude and potential as the ED/Ni75, displayed in Figure S10. The light J–E behavior is suppressed to a similar extent as the ED/Ni75 system. From these results, we deduce that the deleterious interface is due to Ni bonding with the ED hematite surface. We further deduce that the peak observed at ∼1.35 V vs RHE in Figure 2b for the ED/Ni75 system is due to the ED/NiO_y interface states. We therefore focus our attention below on the ED systems.

EIS measurements were performed for bare ED as well as electrodes modified with Ni25 and Ni75 catalysts. Examples of Nyquist plots for ED electrodes measured under illumination at 1, 1.2, and 1.4 V vs. RHE can be seen in Figure S11. At this potential range, two semicircles are clearly visible. The equivalent circuits used to fit the EIS data have been established previously and are shown in Figure S12.[9]

Plots of C_{bulk}, as well as Mott–Schottky (MS) plots prepared from C_{bulk}, are shown in Figure S13 and Figure 3a, respectively. The C_{bulk} behavior was found to be invariant with respect to catalyst under illumination. Dopant densities of 2.40 (±0.14) × 10^{20} cm^{-3}, 2.75 (±0.10) × 10^{20} cm^{-3}, and 2.76 (±0.12) × 10^{20} cm^{-3} were determined for ED/Ni75, ED/Ni25, and bare ED electrodes from fitting the capacitance data to the MS equation[44] using a dielectric constant of 32 for hematite and the geometric surface area of the electrodes.[45] This large dopant density is in good agreement with our previous report of electrodeposited hematite electrodes.[2] The small deviation in dopant density cannot account for the observed behavior for the catalyst coated electrodes. We note that this high dopant density precludes accurate determination of the flat band potential;[46,47] however, the similar behavior of all electrodes indicates that the catalyst does not shift the band positions or affect band bending by pinning the hematite electron Fermi level. This conclusion is further supported by IMPS results discussed below.

The low frequency capacitance is assigned to surface states (C_{ss}) for the bare and the catalyst layers (C_{cat}) for the modified electrodes. The C_{ss}, displayed in Figure 3b, has two peaks. One peak is coincident with the water oxidation onset potential at ∼0.8, which we assign to the water oxidation intermediate species building up on the electrode surface, and a second peak located at more positive potential, ∼1.3 V vs RHE, which we tentatively assign to a surface defect state.[48,49] As shown in Figure 3b, there is an apparent inflection of the J–E curve at this potential which suggests that recombination at this state mitigates the water oxidation efficiency until sufficient potential is applied to deplete the trap of electrons. We note that the presence of two surface states following high temperature annealing procedure is a key difference between the ED and ALD electrodes.[19,20] We therefore hypothesize that this second state is responsible for the dramatically different behavior of catalysts on the ED vs ALD hematite electrodes.

To confirm our assignment and understand the effect of the catalysts, the thickness of catalyst was varied by repeating the deposition procedure one or two additional times to make the series denoted 1, 2, and 3 cycles of catalyst. AFM and ES were utilized to determine the thickness of the catalyst deposited on silicon substrates using comparable procedures. The thickness of the catalyst on hematite electrodes were estimated by integration of the cathodic peaks of the dark J–E (Table S3). For Ni75 catalyst, an approximately linear growth as a function of the number of cycles was measured. Consistent with the experimental values the calculated thickness of the catalyst on hematite was also found to linearly increase with the number of cycles. In addition, the estimated thicknesses via charge integration of modified hematite electrodes were fairly close to the experimentally determined thicknesses of catalyst on silicon substrates by AFM/ES. Any discrepancy in results can be attributed to either the substrate dependence of the growth of the Ni75 catalyst or the possibility that not all the Ni sites are redox active. For Ni25 catalyst, however, the growth mode of the catalyst was found to be nonlinear and the measured thicknesses were generally lower than Ni75 (Table S4). The light and dark J–E curves of the catalyst coated ED electrodes with varying thickness of catalyst are shown in Figure S14. We note at a given potential the photocurrent was diminished by increasing the thickness of the catalyst. This can be understood by considering the illumination direction; the PEC measurements were all performed by illumination from the electrolyte side, thus a portion of the light is lost by competitive light absorption with the catalyst layer. This observation is important since it supports the increasing thickness of catalyst. The parameters derived from fitting the impedance spectra as a function of the catalyst thickness are shown in Figures S15–S18.

The C_{cat} as a function of potential for ED hematite electrodes coated with different thicknesses of Ni25 is compared in Figure 4a. Also shown is the C_{cat} vs potential of Ni25 measured on FTO. Boettcher and co-workers previously studied the electrocatalytic activity of $Ni_{1-x}Fe_xO_y$ as a function of the catalyst loading.[50] It was shown that at the potential range where the catalyst is fully oxidized the C_{cat} was increased with the catalyst loading. As it can be seen from Figure 4a, the C_{cat} increases with increasing the thickness of catalyst, which further indicates that at this condition Ni25 is fully oxidized. The peak

DOI: 10.1021/acs.chemmater.7b01149
Chem. Mater. 2017, 29, 6674–6683

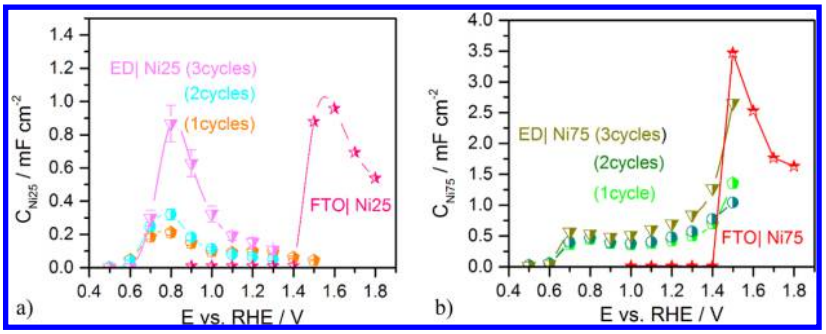

Figure 4. (a) C_{Ni25}, (b) C_{Ni75} obtained from fitting EIS for catalyst coated FTO (1cycle, shown with star symbols) and ED electrodes with varying thickness: 1 cycle (pentagon), 2 cycles (circle), and 3 cycles (triangle).

in C_{cat} is shifted negatively by 0.8 V compared to Ni25 on FTO substrates, indicating 0.8 V of photovoltage is produced by the hematite. Interestingly, this is the exact same photovoltage determined by Wang and co-workers for hematite coated with a $NiFeO_x$ catalyst via open circuit potential measurements.[51] Once the potential of the catalyst drops to more positive potentials via oxidation by photogenerated holes in the hematite, represented by the capacitance, the photocurrent density is controlled by the flux of holes reaching the interface. This behavior is generally consistent with the adaptive junction model, and is further supported by IMPS results described below. We note that the magnitude of the C_{cat} for 1cycle Ni25 on FTO is about 4 times larger than 1cycle Ni25 on ED electrode, suggesting that the catalyst on FTO is thicker. As the thickness of the catalyst increase; however, the C_{cat}(ED) increases and becomes almost equal to the C_{cat}(FTO), which indicates that the growth of the catalyst is substrate dependent, and that the catalyst is fully oxidized.

Figure 4b shows C_{cat} for different nominal thickness of Ni75 on hematite as well as Ni75 on FTO. We note that the peak of C_{cat} for Ni75 on FTO is about 3 times larger than Ni25 on FTO, which is attributed to the expected 3 times larger charge density, which is on the Ni atoms, for a given thickness. The plots of C_{cat} vs potential for Ni75 exhibits three features: (1) similar to the Ni25, there is an onset of C_{cat} at approximately 0.6 V vs RHE; however, instead of reaching a peak, the C_{cat} plateaus over an additional 0.6 V applied potential, (2) where it increases to values consistent with Ni75 on FTO, and (3) the C_{cat} was found to be independent to the thickness of the catalyst at the potential range of 0.7−1.4 V vs RHE. This behavior is consistent with the potential of the catalyst being pinned. Because the bulk capacitance, and thus band bending, band positions and hole flux from hematite, is constant for all ED electrodes measured, the catalyst potential must be controlled by recombination to interface (or catalyst) states. Once these states are emptied, for example by controlling the electron Fermi level (applied potential), the photogenerated holes should further oxidize the catalyst, resulting in an abrupt increase in C_{cat} and current. We assigned the peak observed at ∼1.35 V vs RHE in the J−E curves for the ED/Ni75 system to the interface states, which is coincident with the sudden increase in C_{cat}. This is also approximately the same potential as the second surface state observed for the bare ED electrode displayed in Figure 2b. Thus, we propose that the interface state results from bonding interactions between the ED surface state and Ni hydroxide species.

Further understanding of the effect of catalyst can be gleaned by comparing the trap (recombination) resistance to surface states for the bare, R_{trap}, or catalyst layer for modified electrodes, R_{cat}, and the charge transfer resistance at the respective electrochemical interface, R_{ct}, (Figures S17 and S18). Bisquert and co-workers[52] showed that the R_{trap}/R_{ct} for bare electrodes, which corresponds to R_{cat}/R_{ct} for catalyst coated electrodes, is proportional to the ratio of charge transfer and recombination rate constants. Figure 5 shows the ratio of the

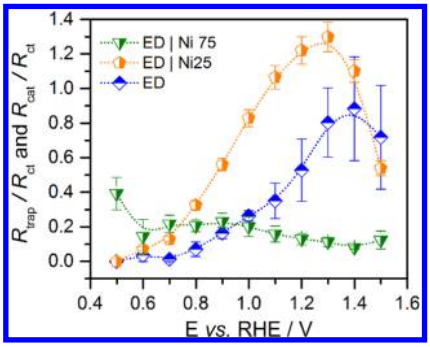

Figure 5. R_{trap}/R_{ct} for bare and R_{cat}/R_{ct} for catalyst modified ED electrodes; bare electrode (blue diamond), Ni75 modified ED electrode (green triangle), and Ni25 coated ED electrode (orange pentagon).

R_{trap}/R_{ct} and R_{cat}/R_{ct} for bare and catalyst modified ED electrodes, respectively. There is a strong correlation between the ratio of resistances to the J−E curves displayed in Figure 2. For the Ni25 coated electrode, improvement in photocurrent and onset potential can be ascribed to an acceleration of charge transfer at the hematite surface compared to the bare electrode. In other words, oxidation of the Ni25 catalyst outcompetes interface recombination to a greater extent than water oxidation competes with surface state recombination at a bare hematite electrode. This result is consistent with our prior report on CoO_x coated hematite electrodes.[53] For Ni75 coated electrodes, on the other hand, the R_{cat}/R_{ct} ratio is low and essentially constant, which indicates that fast recombination at the SC/WOC interface inhibits the photocurrent−voltage behavior.

IMPS measurements were also performed to interrogate the relevant charge dynamics at the surface of the electrode which give rise to the large difference in effects of the Ni25 and Ni75 catalysts. A set of normalized Nyquist plots for bare and modified ED electrodes at 1.3 V vs RHE are shown in Figure S19. Ideally the low frequency intercept (LF) with the real axis is equal to the steady-state photocurrent, which is equal to the rate at which the holes are transferred to the catalysts and from catalyst to solution. At sufficiently high frequencies (HF) the surface recombination is proposed to be frozen out and the HF

DOI: 10.1021/acs.chemmater.7b01149
Chem. Mater. 2017, 29, 6674−6683

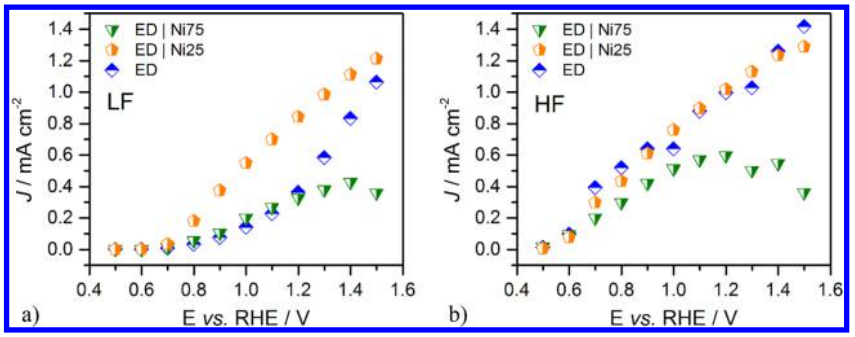

Figure 6. (a) Variation of low frequency (LF), and (b) high frequency (HF) limits of the IMPS response for bare and catalyst coated ED electrodes under monochromatic illumination (470 nm) in contact with 1 M KOH solution; bare electrode (blue diamond), Ni75 modified ED electrode (green triangle), and Ni25 coated ED electrode (orange pentagon).

intercept with real axis thus provides a measure of hole flux toward the SC/electrolyte (or SC/WOC) junction.[54,55] Plots of the LF photocurrent for bare and catalyst coated ED electrodes are compared in Figure 6a. The LF plots mimic the behavior of the $J-E$ plots, consistent with the assignment of the LF as the steady-state photocurrent.

The HF photocurrent is shown in Figure 6b. For the Ni25 modified electrodes, the HF response is nominally identical to that of the bare electrode at all potentials. This indicates that after surface modification with Ni25, the flux of holes to the surface are constant. This is consistent with the Mott−Schottky plots, which show that the energetics at the surface (band edges and band bending) that control the hole flux reaching the interface remains essentially constant. For the Ni75 coated electrode, similar HF responses are observed at potentials ≤1 V vs RHE. At higher potentials, however, the HF response plateaus. This means that either the surface hole flux is constant over a relatively large range of applied potentials, from 1 to 1.5 V vs RHE, or the assignment of the HF is wrong. The validity of the assumption that surface recombination is frozen out at high frequencies obviously depends on the rate of recombination. Just like the bare and Ni25 modified electrodes, the Mott−Schottky plots suggest an increasing hole flux due to increasing band bending over this potential range. The R_{cat}/R_{ct} ratio derived from EIS measurements for the Ni75 electrodes described above suggest fast interfacial recombination, which likewise can explain the HF results. Thus, we assign the plateau region of the HF IMPS results to an essentially constant, fast rate of interfacial recombination process, which is not frozen out.

CONCLUSIONS

The electrocatalytic activity of $Ni_{1-x}Fe_xO_y$ catalysts on FTO substrates and on hematite electrodes in the dark is primarily controlled by the composition of the catalyst, where the nickel-rich Ni75 catalyst is the most active for electrochemical water oxidation. Under illumination, however, several unique differences in the PEC performance of the catalyst modified hematite photoanodes (prepared by ALD and ED) were observed. The PEC performance of the modified ALD electrodes improved upon modification with both Ni25 and Ni75 catalysts, indicated by the ∼200 mV cathodic shift in photocurrent onset potential. Remarkably, the Ni25 (the least active electrocatalyst) modified ALD hematite electrodes performed as good as Ni75 (with superior electrocatalytic activity) coated ALD electrodes. These results further indicate that the overall PEC performance of the catalytically modified electrodes is not only controlled strictly by the electrocatalytic activity of the catalyst.

The most remarkable systems were the modified ED hematite electrodes, where the Ni25 catalyst produced a very large improvement in PEC water oxidation whereas the Ni75 catalyst produced diminished performance. The large improvement of the Ni25 modified ED electrode can be understood by the presence of a surface state defect which influences the $J-E$ behavior of the bare electrode. The Addition of the Ni25 catalyst apparently either passivates this state or just opens a more favorable path of hole transfer to the catalyst which circumvents it. This is supported by the catalyst capacitance which reaches a maximum coincident with the water oxidation onset potential. The capacitance increases with increasing catalyst thickness and illumination intensity, showing it originates from oxidation of the catalyst throughout the entire thickness from photogenerated holes in the hematite. The ratios of R_{cat}/R_{ct} from EIS measurements and HF/LF from IMPS further suggest the improvement in performance derives from an increase in charge separation and reduction in recombination at the hematite surface. These results are generally consistent with modified ALD electrodes,[6,9] and other reported hematite electrode catalyst combinations[51,56] that can be generally interpreted via the adaptive junction model.[18]

The most striking system is Ni75 modified ED hematite electrodes. Independently, they are the best WOC and photoanode examined; however, the combination results in the worst PEC behavior of all systems investigated. The decreased performance coincides with the appearance of an additional capacitive wave. This capacitance is ascribed to an ED hematite−NiO_y interface state that acts as a recombination center. This is supported by the ratio of R_{cat}/R_{ct} from EIS measurements that indicates fast recombination, and the unusual leveling off of the HF intercept of IMPS measurements. The capacitance of the catalyst also remains relatively low and constant over a large potential region, from the nominal $Ni^{3+/2+}$ potential to the interface state potential, indicating the catalyst potential is pinned by the interface state. Thus, even a soft interface that is expected from the deposition of an amorphous metal oxide WOC on hematite under mild conditions can produce states that control the behavior of the junction.

Finally, it is interesting to note that there are prior reports that the PEC water oxidation is influenced by surface or interface states, which can be perhaps better understood following the insight provided here.[19,20] Wang and co-workers,[21] showed that the surface modification of hematite

DOI: 10.1021/acs.chemmater.7b01149
Chem. Mater. 2017, 29, 6674−6683

through a regrowth procedure followed by $NiFeO_y$ catalyst coating resulted in a substantial improvement of the photoanode performance. This result is analogous to what we observe with the ED/Ni25 junction. Li and co-workers studied $Ni(OH)_2$ coated Fe_2O_3 nanowires.[57] They observed that coating the hematite electrode with $Ni(OH)_2$ resulted in an initial cathodic shift of the photocurrent density; however, the photocurrent decayed by ~90%, to values lower than the bare hematite, within 30 s. This behavior was attributed to the fast oxidation of Ni^{2+} to Ni^{3+}, followed by a rate limiting step of further oxidation to a Ni^{4+} species, thus resulting in the NiOOH film storing charge but not producing a sustained enhancement of water oxidation. This result can be understood by the NiOOH catalyst being pinned, thus not achieving a potential sufficient to sustain water oxidation, consistent with what we observe with the ED/Ni75 (and NiO_y) system. In another system, Choi and co-workers[58] showed that the PEC characteristic of $BiVO_4$ is substantially improved when the interface between the semiconductor and NiOOH, was modified with FeOOH. This result is consistent with our findings that the Ni25, which consists of separate FeOOH and Fe-doped NiOOH phases, passivates the ED hematite interface. These examples emphasize the importance of the SC/WOC interface, where the contact of a Ni-rich phase with otherwise promising photoanode materials may produce a large density of deleterious states that act as recombination centers. Clearly, more research is needed to understand such phenomena in more detail to develop more general models of this important interface.

■ ASSOCIATED CONTENT

Supporting Information

The Supporting Information is available free of charge on the ACS Publications website at DOI: 10.1021/acs.chemmater.7b01149.

Experimental conditions, SEM image, Raman spectroscopy, raw and fitted detailed XPS spectra of the catalyst with varying composition, *J*–*E* curves, EIS equivalent circuit and fitted parameters, thickness of the catalysts (PDF)

■ AUTHOR INFORMATION

Corresponding Author

*T. W. Hamann. E-mail: hamann@chemistry.msu.edu.

ORCID

Thomas W. Hamann: 0000-0001-6917-7494

Notes

The authors declare no competing financial interest.

■ ACKNOWLEDGMENTS

T.W.H. thanks the National Science Foundation (CHE-1664823) for the support of this research. H.H. thanks the Environmental Science and Policy Program at Michigan State University for partial support of this research. We thank Prof. Boettcher for his insightful comments during the preparation of this manuscript.

■ REFERENCES

(1) Hamann, T. W. Splitting Water with Rust: Hematite Photoelectrochemistry. *Dalt. Trans.* **2012**, *41* (26), 7830–7834.

(2) Zandi, O.; Schon, A. R.; Hajibabaei, H.; Hamann, T. W. Enhanced Charge Separation and Collection in High-Performance Electrodeposited Hematite Films. *Chem. Mater.* **2016**, *28* (3), 765–771.

(3) Klahr, B. M.; Hamann, T. W. Current and Voltage Limiting Processes in Thin Film Hematite Electrodes. *J. Phys. Chem. C* **2011**, *115* (16), 8393–8399.

(4) Klahr, B. M.; Martinson, A. B. F.; Hamann, T. W. Photoelectrochemical Investigation of Ultrathin Film Iron Oxide Solar Cells Prepared by Atomic Layer Deposition. *Langmuir* **2011**, *27* (1), 461–468.

(5) Deng, J.; Lv, X.; Zhang, H.; Zhao, B.; Sun, X.; Zhong, J. Loading the FeNiOOH Cocatalyst on Pt-Modified Hematite Nanostructures for Efficient Solar Water Oxidation. *Phys. Chem. Chem. Phys.* **2016**, *18* (15), 10453–10458.

(6) Young, K. M. H.; Hamann, T. W. Enhanced Photocatalytic Water Oxidation Efficiency with Ni(OH) 2 Catalysts Deposited on α-Fe 2 O 3 via ALD. *Chem. Commun.* **2014**, *50* (63), 8727–8730.

(7) Upul Wijayantha, K. G.; Saremi-Yarahmadi, S.; Peter, L. M. Kinetics of Oxygen Evolution at α-Fe2O3 Photoanodes: A Study by Photoelectrochemical Impedance Spectroscopy. *Phys. Chem. Chem. Phys.* **2011**, *13* (12), 5264–5270.

(8) Gamelin, D. R. Water Splitting: Catalyst or Spectator? *Nat. Chem.* **2012**, *4* (12), 965–967.

(9) Klahr, B.; Gimenez, S.; Fabregat-Santiago, F.; Bisquert, J.; Hamann, T. W. Photoelectrochemical and Impedance Spectroscopic Investigation of Water Oxidation with "Co-Pi"-Coated Hematite Electrodes. *J. Am. Chem. Soc.* **2012**, *134* (40), 16693–16700.

(10) McDonald, K. J.; Choi, K.-S. Photodeposition of Co-Based Oxygen Evolution Catalysts on α-Fe $_2$ O $_3$ Photoanodes. *Chem. Mater.* **2011**, *23* (7), 1686–1693.

(11) Du, C.; Yang, X.; Mayer, M. T.; Hoyt, H.; Xie, J.; McMahon, G.; Bischoping, G.; Wang, D. Hematite-Based Water Splitting with Low Turn-on Voltages. *Angew. Chem., Int. Ed.* **2013**, *52* (48), 12692–12695.

(12) Zhong, D. K.; Choi, S.; Gamelin, D. R. Near-Complete Suppression of Surface Recombination in Solar Photoelectrolysis by "Co-Pi" Catalyst-Modified W:BiVO $_4$. *J. Am. Chem. Soc.* **2011**, *133* (45), 18370–18377.

(13) Liu, R.; Zheng, Z.; Spurgeon, J.; Yang, X. Enhanced Photoelectrochemical Water-Splitting Performance of Semiconductors by Surface Passivation Layers. *Energy Environ. Sci.* **2014**, *7* (8), 2504–2517.

(14) Barroso, M.; Cowan, A. J.; Pendlebury, S. R.; Grätzel, M.; Klug, D. R.; Durrant, J. R. The Role of Cobalt Phosphate in Enhancing the Photocatalytic Activity of α-Fe $_2$ O $_3$ toward Water Oxidation. *J. Am. Chem. Soc.* **2011**, *133* (38), 14868–14871.

(15) Barroso, M.; Mesa, C. A.; Pendlebury, S. R.; Cowan, A. J.; Hisatomi, T.; Sivula, K.; Gratzel, M.; Klug, D. R.; Durrant, J. R. Dynamics of Photogenerated Holes in Surface Modified -Fe2O3 Photoanodes for Solar Water Splitting. *Proc. Natl. Acad. Sci. U. S. A.* **2012**, *109* (39), 15640–15645.

(16) Zhong, D. K.; Sun, J.; Inumaru, H.; Gamelin, D. R. Solar Water Oxidation by Composite Catalyst/α-Fe $_2$ O $_3$ Photoanodes. *J. Am. Chem. Soc.* **2009**, *131* (17), 6086–6087.

(17) Lin, F.; Boettcher, S. W. Adaptive Semiconductor/electrocatalyst Junctions in Water-Splitting Photoanodes. *Nat. Mater.* **2013**, *13* (1), 81–86.

(18) Nellist, M. R.; Laskowski, F. A. L.; Lin, F.; Mills, T. J.; Boettcher, S. W. Semiconductor–Electrocatalyst Interfaces: Theory, Experiment, and Applications in Photoelectrochemical Water Splitting. *Acc. Chem. Res.* **2016**, *49* (4), 733–740.

(19) Klahr, B.; Gimenez, S.; Fabregat-Santiago, F.; Hamann, T.; Bisquert, J. Water Oxidation at Hematite Photoelectrodes: The Role of Surface States. *J. Am. Chem. Soc.* **2012**, *134* (9), 4294–4302.

(20) Zandi, O.; Hamann, T. W. Enhanced Water Splitting Efficiency Through Selective Surface State Removal. *J. Phys. Chem. Lett.* **2014**, *5* (9), 1522–1526.

(21) Jang, J.-W.; Du, C.; Ye, Y.; Lin, Y.; Yao, X.; Thorne, J.; Liu, E.; McMahon, G.; Zhu, J.; Javey, A.; Guo, J.; Wang, D. Enabling

DOI: 10.1021/acs.chemmater.7b01149
Chem. Mater. 2017, 29, 6674–6683

Unassisted Solar Water Splitting by Iron Oxide and Silicon. *Nat. Commun.* **2015**, *6*, 7447.
(22) Trześniewski, B. J.; Smith, W. A. Photocharged BiVO 4 Photoanodes for Improved Solar Water Splitting. *J. Mater. Chem. A* **2016**, *4* (8), 2919−2926.
(23) Liu, G.; Ye, S.; Yan, P.; Xiong, F.; Fu, P.; Wang, Z.; Chen, Z.; Shi, J.; Li, C. Enabling an Integrated Tantalum Nitride Photoanode to Approach the Theoretical Photocurrent Limit for Solar Water Splitting. *Energy Environ. Sci.* **2016**, *9* (4), 1327−1334.
(24) Le Formal, F.; Pendlebury, S. R.; Cornuz, M.; Tilley, S. D.; Grätzel, M.; Durrant, J. R. Back Electron−Hole Recombination in Hematite Photoanodes for Water Splitting. *J. Am. Chem. Soc.* **2014**, *136* (6), 2564−2574.
(25) Kim, J. Y.; Magesh, G.; Youn, D. H.; Jang, J.-W.; Kubota, J.; Domen, K.; Lee, J. S. Single-Crystalline, Wormlike Hematite Photoanodes for Efficient Solar Water Splitting. *Sci. Rep.* **2013**, *3*, 2681.
(26) Morales-Guio, C. G.; Mayer, M. T.; Yella, A.; Tilley, S. D.; Grätzel, M.; Hu, X. An Optically Transparent Iron Nickel Oxide Catalyst for Solar Water Splitting. *J. Am. Chem. Soc.* **2015**, *137* (31), 9927−9936.
(27) Louie, M. W.; Bell, A. T. An Investigation of Thin-Film Ni-Fe Oxide Catalysts for the Electrochemical Evolution of Oxygen. *J. Am. Chem. Soc.* **2013**, *135* (33), 12329−12337.
(28) Friebel, D.; Louie, M. W.; Bajdich, M.; Sanwald, K. E.; Cai, Y.; Wise, A. M.; Cheng, M.-J.; Sokaras, D.; Weng, T.-C.; Alonso-Mori, R.; Davis, R. C.; Bargar, J. R.; Nørskov, J. K.; Nilsson, A.; Bell, A. T. Identification of Highly Active Fe Sites in (Ni,Fe)OOH for Electrocatalytic Water Splitting. *J. Am. Chem. Soc.* **2015**, *137* (3), 1305−1313.
(29) Trotochaud, L.; Young, S. L.; Ranney, J. K.; Boettcher, S. W. Nickel-Iron Oxyhydroxide Oxygen-Evolution Electrocatalysts: The Role of Intentional and Incidental Iron Incorporation. *J. Am. Chem. Soc.* **2014**, *136* (18), 6744−6753.
(30) Burke, M. S.; Enman, L. J.; Batchellor, A. S.; Zou, S.; Boettcher, S. W. Oxygen Evolution Reaction Electrocatalysis on Transition Metal Oxides and (Oxy)hydroxides: Activity Trends and Design Principles. *Chem. Mater.* **2015**, *27* (22), 7549−7558.
(31) Zandi, O.; Beardslee, J. A.; Hamann, T. Substrate Dependent Water Splitting with Ultrathin α-Fe $_2$ O $_3$ Electrodes. *J. Phys. Chem. C* **2014**, *118* (30), 16494−16503.
(32) Dezelah, C. L.; Niinistö, J.; Arstila, K.; Niinistö, L.; Winter, C. H. Atomic Layer Deposition of Ga 2 O 3 Films from a Dialkylamido-Based Precursor. *Chem. Mater.* **2006**, *18* (2), 471−475.
(33) Klahr, B. M.; Martinson, A. B. F.; Hamann, T. W. Photoelectrochemical Investigation of Ultrathin Film Iron Oxide Solar Cells Prepared by Atomic Layer Deposition. *Langmuir* **2011**, *27* (1), 461−468.
(34) Smith, R. D. L.; Prevot, M. S.; Fagan, R. D.; Zhang, Z.; Sedach, P. A.; Siu, M. K. J.; Trudel, S.; Berlinguette, C. P. Photochemical Route for Accessing Amorphous Metal Oxide Materials for Water Oxidation Catalysis. *Science (Washington, DC, U. S.)* **2013**, *340* (6128), 60−63.
(35) Hilfiker, J. N.; Singh, N.; Tiwald, T.; Convey, D.; Smith, S. M.; Baker, J. H.; Tompkins, H. G. Survey of Methods to Characterize Thin Absorbing Films with Spectroscopic Ellipsometry. *Thin Solid Films* **2008**, *516* (22), 7979−7989.
(36) Klaus, S.; Louie, M. W.; Trotochaud, L.; Bell, A. T. Role of Catalyst Preparation on the Electrocatalytic Activity of Ni 1− X Fe X OOH for the Oxygen Evolution Reaction. *J. Phys. Chem. C* **2015**, *119* (32), 18303−18316.
(37) Swierk, J. R.; Klaus, S.; Trotochaud, L.; Bell, A. T.; Tilley, T. D. Electrochemical Study of the Energetics of the Oxygen Evolution Reaction at Nickel Iron (Oxy)Hydroxide Catalysts. *J. Phys. Chem. C* **2015**, *119* (33), 19022−19029.
(38) Klaus, S.; Cai, Y.; Louie, M. W.; Trotochaud, L.; Bell, A. T. Effects of Fe Electrolyte Impurities on Ni(OH) 2 /NiOOH Structure and Oxygen Evolution Activity. *J. Phys. Chem. C* **2015**, *119* (13), 7243−7254.
(39) Smith, R. D. L.; Prévot, M. S.; Fagan, R. D.; Trudel, S.; Berlinguette, C. P. Water Oxidation Catalysis: Electrocatalytic Response to Metal Stoichiometry in Amorphous Metal Oxide Films Containing Iron, Cobalt, and Nickel. *J. Am. Chem. Soc.* **2013**, *135* (31), 11580−11586.
(40) Trudel, S.; Daryl Crozier, E.; Gordon, R. A.; Budnik, P. S.; Hill, R. H. X-Ray Absorption Fine Structure Study of Amorphous Metal Oxide Thin Films Prepared by Photochemical Metalorganic Deposition. *J. Solid State Chem.* **2011**, *184* (5), 1025−1035.
(41) Andronic, L. S.; Hill, R. H. The Mechanism of the Photochemical Metal Organic Deposition of Lead Oxide Films from Thin Films of Lead (II) 2-Ethylhexanoate. *J. Photochem. Photobiol., A* **2002**, *152* (1), 259−265.
(42) Klahr, B.; Gimenez, S.; Fabregat-Santiago, F.; Bisquert, J.; Hamann, T. W. Photoelectrochemical and Impedance Spectroscopic Investigation of Water Oxidation with "Co−Pi"-Coated Hematite Electrodes. *J. Am. Chem. Soc.* **2012**, *134* (40), 16693−16700.
(43) Young, K. M. H.; Hamann, T. W. Enhanced Photocatalytic Water Oxidation Efficiency with Ni(OH)2 Catalysts Deposited on α-Fe2O3via ALD. *Chem. Commun. (Cambridge, U. K.)* **2014**, *50* (63), 8727−8730.
(44) Gelderman, K.; Lee, L.; Donne, S. W. Flat-Band Potential of a Semiconductor: Using the Mott−Schottky Equation. *J. Chem. Educ.* **2007**, *84* (4), 685−688.
(45) Glasscock, J. A.; Barnes, P. R. F.; Plumb, I. C.; Bendavid, A.; Martin, P. J. Structural, Optical and Electrical Properties of Undoped Polycrystalline Hematite Thin Films Produced Using Filtered Arc Deposition. *Thin Solid Films* **2008**, *516* (8), 1716−1724.
(46) Gomes, W. P.; Cardon, F. Electron Energy Levels in Semiconductor Electrochemistry. *Prog. Surf. Sci.* **1982**, *12* (2), 155−215.
(47) van den Meerakker, J. E. A. M.; Meulenkamp, E. A.; Scholten, M. (Photo)electrochemical Characterization of Tin-doped Indium Oxide. *J. Appl. Phys.* **1993**, *74* (5), 3282−3288.
(48) Klahr, B.; Gimenez, S.; Fabregat-Santiago, F.; Hamann, T.; Bisquert, J. Water Oxidation at Hematite Photoelectrodes: The Role of Surface States. *J. Am. Chem. Soc.* **2012**, *134* (9), 4294−4302.
(49) Klahr, B.; Hamann, T. Water Oxidation on Hematite Photoelectrodes: Insight into the Nature of Surface States through In Situ Spectroelectrochemistry. *J. Phys. Chem. C* **2014**, *118* (19), 10393−10399.
(50) Batchellor, A. S.; Boettcher, S. W. Pulse-Electrodeposited Ni−Fe (Oxy)hydroxide Oxygen Evolution Electrocatalysts with High Geometric and Intrinsic Activities at Large Mass Loadings. *ACS Catal.* **2015**, *5* (11), 6680−6689.
(51) Thorne, J. E.; Li, S.; Du, C.; Qin, G.; Wang, D. Energetics at the Surface of Photoelectrodes and Its Influence on the Photoelectrochemical Properties. *J. Phys. Chem. Lett.* **2015**, *6* (20), 4083−4088.
(52) Bertoluzzi, L.; Bisquert, J. Equivalent Circuit of Electrons and Holes in Thin Semiconductor Films for Photoelectrochemical Water Splitting Applications. *J. Phys. Chem. Lett.* **2012**, *3* (17), 2517−2522.
(53) Riha, S. C.; Klahr, B. M.; Tyo, E. C.; Seifert, S.; Vajda, S.; Pellin, M. J.; Hamann, T. W.; Martinson, A. B. F. Atomic Layer Deposition of a Submonolayer Catalyst for the Enhanced Photoelectrochemical Performance of Water Oxidation with Hematite. *ACS Nano* **2013**, *7* (3), 2396−2405.
(54) Ponomarev, E. A.; Peter, L. M. A Generalized Theory of Intensity Modulated Photocurrent Spectroscopy (IMPS). *J. Electroanal. Chem.* **1995**, *396* (1−2), 219−226.
(55) Peter, L. M.; Wijayantha, K. G. U.; Tahir, A. A. Kinetics of Light-Driven Oxygen Evolution at α-Fe 2 O 3 Electrodes. *Faraday Discuss.* **2012**, *155* (0), 309−322.
(56) Thorne, J. E.; Jang, J.-W.; Liu, E. Y.; Wang, D. Understanding the Origin of Photoelectrode Performance Enhancement by Probing Surface Kinetics. *Chem. Sci.* **2016**, *7* (5), 3347−3354.
(57) Wang, G.; Ling, Y.; Lu, X.; Zhai, T.; Qian, F.; Tong, Y.; Li, Y. A Mechanistic Study into the Catalytic Effect of Ni(OH)2 on Hematite

DOI: 10.1021/acs.chemmater.7b01149
Chem. Mater. 2017, 29, 6674−6683

for Photoelectrochemical Water Oxidation. *Nanoscale* **2013**, *5* (10), 4129−4133.
(58) Kim, T. W.; Choi, K.-S. Nanoporous BiVO4 Photoanodes with Dual-Layer Oxygen Evolution Catalysts for Solar Water Splitting. *Science* **2014**, *343* (6174), 990−994.

DOI: 10.1021/acs.chemmater.7b01149
Chem. Mater. 2017, 29, 6674−6683